Film Cooling in a Separated Flow Field on a Novel Lightweight Turbine Blade

Yoji Okita

Chiyuki Nakamata

Aero-Engine and Space Operations,
IHI Corporation,
Tokyo 190-1297, Japan

Masaya Kumada
Department of Mechanical Engineering,
Gifu University,
Gifu 501-1193, Japan

Masahiro Ikeda
Institute of Industrial Science,
University of Tokyo,
Tokyo 153-8505, Japan

The primary contribution of this research is to clarify the feasibility of a novel lightweight turbine blade with internal and external cooling, which is invented, aiming at drastic reduction in weight. With a considerably thinner airfoil, an extensive separation bubble is formed on the pressure side, and film cooling performance in such a flow field has to be investigated. Experimental results with a curved duct setup, which simulates the flow field around the proposed airfoil, show that a film cooling is still an effective measure of cooling even in the vastly separated region, and it behaves quite similarly to the conventional correlation, except for lower blowing ratios, where the thermal field is strongly affected by the intense recirculation flow. Comparisons between the experimental and numerical results verify that an affordable Reynolds-averaged Navier–Stokes simulation is useful to investigate the detailed physics of this flow field. With the numerical modeling, a cooling performance of the proposed blade under a typical engine operating condition is simulated, and the metal temperatures of the blade are also predicted with a fluid-solid conjugate calculation. The resultant thermal distribution in the airfoil suggests that the trailing edge portion is inevitably most critical in the temperature, and also a considerable thermal gradient across the blade is induced. Thermal profile, however, is partly recovered with some of the film coolant being bypassed from the pressure side to the suction side. [DOI: 10.1115/1.3144165]

1 Introduction

Nowadays, in the aero-engine industry, there is an increasing demand for even higher performance and drastic reduction in engine weight while meeting the safety and reliability requirements. In order to achieve higher efficiency, typical engine operating temperatures were pushed much higher than the allowable turbine airfoil metal temperatures. This necessitates more complicated and intensive cooling measures, especially for high-pressure turbine, to provide thermal protection to the airfoils, which often bring about an increase in manufacturing and/or repair costs. On the other hand, driven by the need of weight reduction, much thinner blades with large separation bubble on the airfoil pressure side were studied (e.g., Ref. [1]). Investigations of such thin airfoils application, however, were limited for uncooled turbine blade so far (typically for low-pressure turbines).

Given this background, the authors' group is motivated to seek a novel concept, which realizes the drastic weight reduction for the cooled turbine blade without any penalties on performance or manufacturing cost. One of the newly devised cooling concepts, which leads to a strikingly thinner cooled blade [2], is achieved by removing considerable portion of the airfoil body from the pressure side (Fig. 1). The blade forms a characteristic step on the pressure surface with film cooling injection. Air can be ejected through slots or discrete holes to generate a cooling film on the pressure-side wall. The suction side is also covered by the coolant injected from the film holes located upstream, and optionally by extra coolant bypassed from the pressure side through discrete holes to protect the thermally stressed trailing edge region.

The straightforward benefit of this concept is a weight reduction in the rotating blades themselves. Reduction in the blade weight results in much more significant reduction in the turbine disk weight and/or allows a less expensive material to be applied to the disk. Light turbine rotor is able to increase the critical speed of the whole engine rotor system beyond the operating range, which produces a great benefit for the aero-engine users. The weight reduction is not all this invention brings about. It also greatly simplifies the internal cooling passages of the blade, which is desirable from the manufacturability and repairability point of view.

One of the technological challenges in the proposed concept is definitely a control of flow and thermal field along the vastly separated pressure side. There are many papers in the open literature that deal with film cooling in a separated flow downstream of a backward-facing step, which is typically encountered in turbine airfoil trailing edge cutback [3–9]. In such a flow field, it was well established that the coolant to the mainflow blowing ratio, density ratio, lip thickness, and angle of injection are the key parameters. The slot lip thickness to height ratio (t/s) is reported to have a great impact on the film effectiveness. The past works for relatively smaller t/s range ($t/s<2.0$) showed that the film effectiveness decreases as the lip thickness increases [3]. They claimed that the mixing between the mainflow and the coolant is minimized for very small lip thickness, whereas it increases as the lip thickness gets large, resulting in lower film effectiveness.

The flow field on the pressure side of the proposed thinner airfoil with film cooling is analogous to these past works except for much higher t/s ratio. To evaluate the feasibility of cooling performance in a large separation bubble, the authors' group previously investigated the adiabatic film effectiveness in a separated flow downstream of a backward-facing step with large lip thickness (up to $t/s=8$) [10]. The key finding of the previous study is that the film cooling flow behaves as a wall jet with such a large lip thickness, and the film effectiveness does not considerably deteriorate as suggested from the data for smaller t/s case.

The present work aims at taking a step further toward the realization of the proposed concept. The first contribution of the present paper is to study a separated flow field with film cooling in a curved duct experiment, which is designed to mimic the pro-

Contributed by the International Gas Turbine Institute of ASME for publication in the JOURNAL OF TURBOMACHINERY. Manuscript received July 14, 2008; final manuscript received March 9, 2009; published online March 24, 2010. Review conducted by David Wisler. Paper presented at the ASME Turbo Expo 2008: Land, Sea and Air (GT2008), Berlin, Germany, June 9–13, 2008.

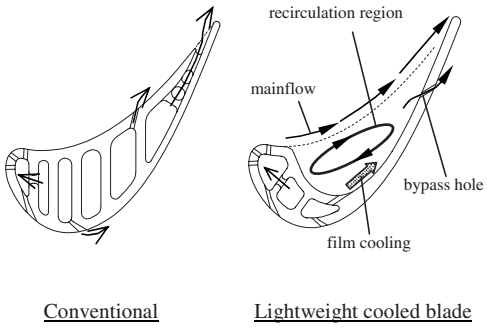

Fig. 1 Sketch of the lightweight cooled blade

posed lightweight blade airfoil even more faithfully. Numerical calculation is also carried out to understand the details of the heat and the fluid flow. The calculation is compared with the experimental data to verify its applicability to such a unique flow field, and hopefully, to the design optimization in future. Another contribution of this paper is that the cooling performance of the proposed blade under a typical engine operating condition is predicted by the numerical method. On the whole, the scope and aim of the present paper are to clarify the feasibility of the novel lightweight blade concept with more realistic geometries and in more realistic flow conditions.

The experimental and numerical methodologies for the curved duct setup are first briefly outlined in the next section. After the presentation of the results and the discussions with this fundamental duct case, the calculated flow and thermal fields under an engine operating condition are described in the Sec. 3. Finally the main conclusions are summarized in the Sec. 4.

2 Flow and Thermal Field in a Curved Duct

2.1 Experimental Setup. The tests are performed in a wind tunnel facility shown in Fig. 2. The mainflow air is pressurized by a blower (Hitachi VB-040-E). The compressed air goes through a flowmeter, a plenum chamber, and a straight duct before it enters the curved duct test section. Another compressed air is used for the film cooling fluid and is supplied through a separate duct into the test section. Laminar flowmeters (Sokken LFE-50B/-150B) and thermocouples are mounted in the mainflow and in the cooling supply line to measure and control the flow rates and the temperatures. Downstream of the test section, the flow discharges to the atmosphere.

Figure 3 shows a cross-sectional view of the test section. The key dimensions and the flow parameters in the experiment are listed in Table 1, where values expected in a typical operating HP-turbine are also shown. The entry straight part of the test section has a height of 45.5 mm and a width of 120 mm. The duct profile of the curved section is intended to simulate the suction

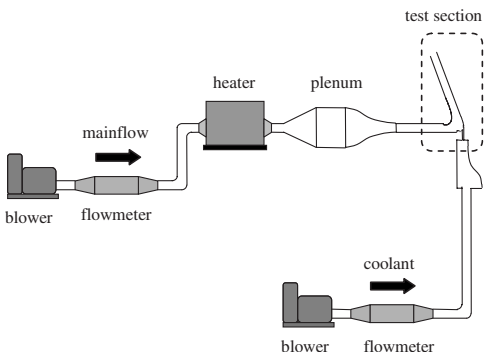

Fig. 2 General arrangement of the facility

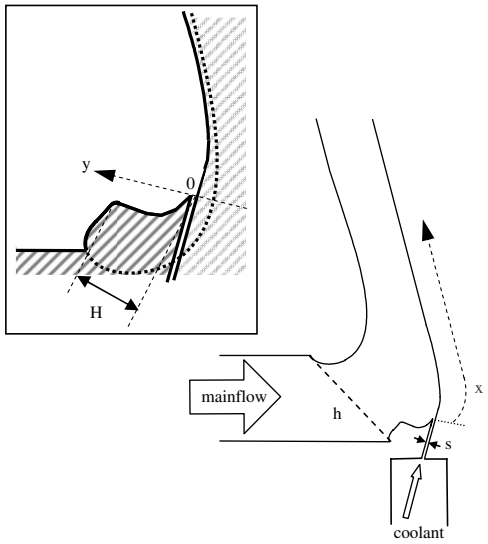

Fig. 3 Schematic of the curved duct test section

and the pressure surface of the proposed lightweight turbine blade. The profile is completely consistent with the airfoil shape investigated under an engine-representative flow condition discussed in the Sec. 3. A slot for film ejection is positioned at the bottom of the curvature, and the direction of the ejection is set tangential to the mainflow passage at the slot opening. The step height to the slot height ratio (H/S) in the present experiment is identical with the slot lip thickness to the slot height ratio (t/s) in the authors' previous straight duct experiment [10]. These geometrical settings are also intended to reproduce the key aspects of the proposed airfoil geometry and the cooling strategy shown in Fig. 1.

By controlling the inverters installed in each blower, the desired Reynolds number can be attained. The mainflow temperature is increased by a heater before it enters the plenum. The tests are carried out by holding all flow parameters constant throughout the run except the coolant flow rate, as listed in Table 1. Three different blowing ratios (0.3, 1.0, and 2.0) were examined in the present experiment. As shown in Table 1, the test conditions were able to model the flow field expected in the typical aero-engines, though the density ratio cannot be matched. For each blowing ratio, sufficient time is allowed for the system to reach equilibrium, at which time a series of temperature measurements are recorded at each instrumentation location, and reduced immediately in a data acquisition PC. The slot cooling flow is then increased for a larger blowing ratio, and data are recorded again. This process is repeated until measurements are obtained for a whole range of blowing ratio.

The mainflow air temperature (T_g) is measured with a thermocouple located 10 mm upstream of the test section inlet, though the spatial variation is not measured. However, the plenum chamber has a structure to flatten the flow; therefore, the temperature

Table 1 Key dimensions and flow parameters in the curved duct experiment

	Present	Typical in engine
w/h	2.6	-
h/H	5.7	-
H/S	8.0	-
Re_s	$3.0\times10^2-2.0\times10^3$	10^3-10^4
Re_θ	300	10^2-10^3
ρ_c/ρ_g	1.1	1.2–2.0
M	0.3, 1.0, 2.0	<2.0

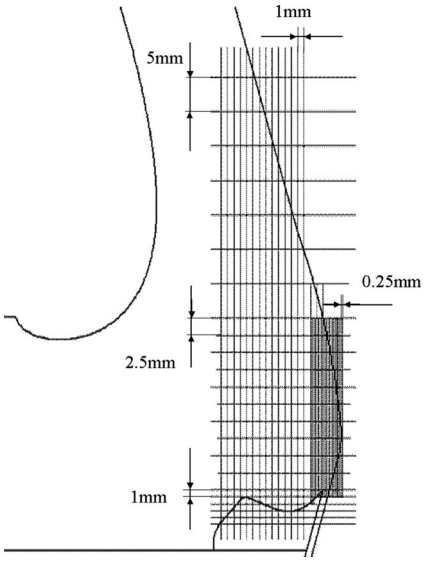

Fig. 4 Thermocouple locations for the fluid temperature traverse

profile can be assumed practically uniform. The temperature of the slot coolant flow (T_c) is also measured upstream of the slot opening. These mainflow and coolant temperatures are used as reference temperatures when adiabatic film effectiveness is defined. In order to measure the adiabatic surface temperatures on the curved duct wall, where the film coolant issues, T-type thermocouples are embedded at intervals of 5 mm with the slot opening edge as a starting point. These surface temperatures are only measured along the centerline of the test section. Also the spatial thermal field in the region of main interest is measured by traversing a T-type thermocouple. The measurement grid is shown in Fig. 4. The traverse is carried out only in the center plane of the duct.

The current test section does not have a turbulence grid in the mainstream passage, and the turbulence intensity is estimated to be about 3% based on the experience of previous similar tests.

Uncertainties in the measurement are calculated using the method of Kline and McClintock [11]. The overall uncertainty for the adiabatic film effectiveness is found to be $\pm 5\%$. The uncertainty in the measured mainflow rate is $\pm 2.5\%$. The uncertainty for the coolant flow rate is $\pm 2\%$ at the highest blowing flow rate. The uncertainty of the temperature in the duct flow field is $\pm 4\%$.

2.2 Numerical Method. The aim of the numerical investigation is to give physical insight into the mechanism of interaction between the mainflow and the film jet, especially in the vastly separated flow field, where the main interest of the present work exists.

The compressible Reynolds-averaged Navier–Stokes (RANS) equations are solved using a pressure correction method with the FLUENT 6 software [12]. The calculations are two-dimensional for the curved duct experimental setup. The equations are discretized using a finite volume method with the convective variables being resolved in a second-order upwind scheme. The turbulent stresses and heat fluxes are modeled through the realizable k-epsilon model with the enhanced wall treatment (a low Reynolds number model) at near-wall cells. The calculations are all steady-state. Convergence of the iterative steady-state solution is declared when reductions in normalized residuals of at least three orders of magnitude with leveling-off of the residuals are achieved for all the solution variables.

The computational domain for the curved duct (Fig. 5) includes the mainflow, the film slot, and the coolant plenum (note that every three or four grid lines are presented in Fig. 5(*a*) to simplify the picture). All the boundary conditions are consistent with the

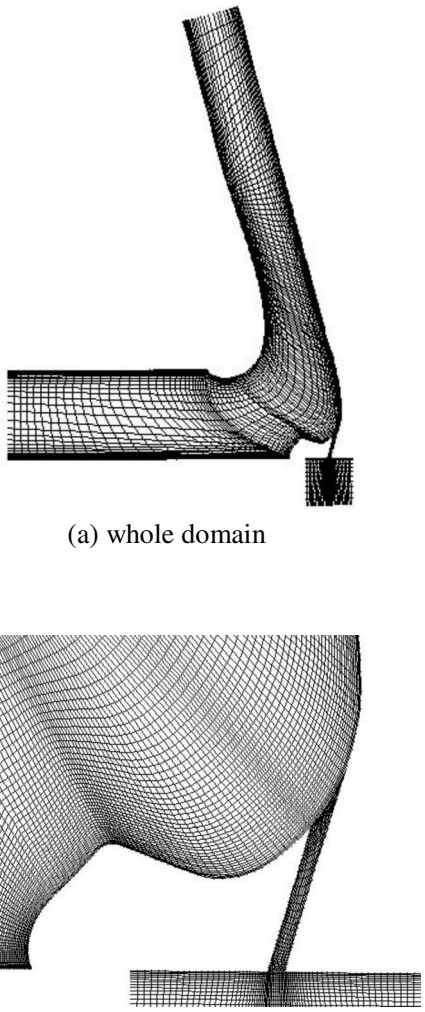

(a) whole domain

(b) details near the injection

Fig. 5 Computational domain and mesh

experimental setup. No-slip and adiabatic conditions are applied on the solid surfaces. At the coolant plenum inlet, the mass flux is set uniformly so as to give the required mass flow, and the temperature is set at the coolant supply temperature. In the mainflow, the mass flow rate and the temperature are specified at the inlet. The turbulent kinetic energy is set with a turbulence intensity of 3%, and the dissipation rate then obtained assuming turbulence Reynolds number equal to 100. At the flow exit, the static pressure is specified, and the other variables are extrapolated from the interior of the solution domain.

The number of control volume cells is about 3×10^4. The converged solutions have near-wall mesh y^+ values less than 5 in most regions, which is within a recommended criteria with the enhanced wall treatment. A finer 1.2×10^5 mesh is also tested for grid sensitivity comparisons. The streamwise distributions of film effectiveness obtained with the two grids are practically identical, as shown in Fig. 6. In the subsequent plots, the results with 3×10^4 mesh are presented.

2.3 Results and Discussions. Prior to addressing the thermal field, a basic aerodynamic validity of the curved duct setup is first discussed. In the experiment, the static pressure along the duct surface is not measured. To evaluate whether the present experimental setup produces the desired flow field, the static pressure coefficient along the surface obtained from the numerical results are compared in Fig. 7 between the curved duct and the actual

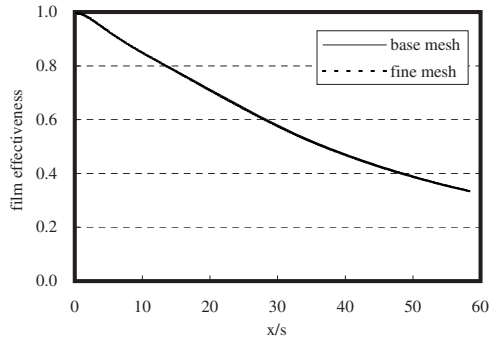

Fig. 6 Comparison of streamwise distribution of calculated film effectiveness with the two grids for $M=1.0$

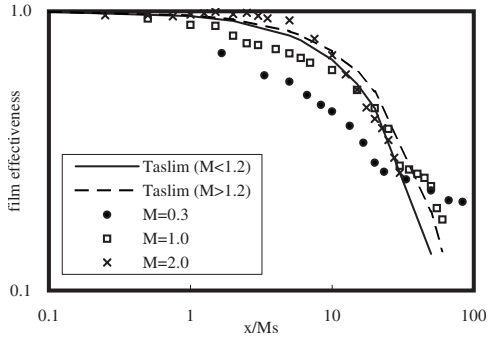

Fig. 9 Comparison of the streamwise profile of film effectiveness between the present data and the correlation by Taslim et al. [3]

blade passage described in the next section. For the suction surface, there is clearly a difference in the front part acceleration. For the pressure surface, where the main interest of the present work exists, the curved duct setup reproduces fairly well the distribution expected in the blade-to-blade passage under the engine condition, though the acceleration in the rear part is a bit steeper.

The comparisons of local adiabatic film effectiveness (η_f) along the centerline of the duct surface are made between various blowing ratios (M). The distribution of η_f with coordinate along the surface from the slot opening is shown in Fig. 8.

Close to the slot exit, the effectiveness is at its maximum and it decreases with the streamwise distance from the slot exit, as a natural consequence of mixing with the mainflow.

It is found that the effectiveness is a monotonically increasing function of M within the investigated range of the experiment. This trend is similar to the one observed in the authors' previous work, where the flow downstream of a backward-facing step was studied [10]. In that study, the detailed flow and thermal field measurement revealed that the coolant injected from the slot behaves as a wall jet, and that observation was considered reasonable because such a flow field is expected to show a monotonically increasing relationship between η_f and M. The trend shown in the Fig. 8 suggests that the similar mechanics governs the present flow field.

The curve for the $M=0.3$ case does not attain unity even at the slot exit. This suggests that the flow mixing has started inside the slot. Several past works also reported similar behavior in case of low velocity ratios [13–15]. Also, this case exhibits a rapid mixing within the first ten slot height distance, which is not observed in the other higher blowing ratio cases.

The $M=2.0$ case shows a characteristic behavior near the slot exit, where the effectiveness slightly drops just downstream of the exit, then recovers again to almost unity, and finally, it starts to decrease monotonically as same as in the other blowing ratio cases. This behavior is not captured in the numerical simulation. There is a possibility that a small separation occurs just at the slot exit, followed by a quick reattachment downstream, which cannot be resolved by the present numerical method.

The experimental results of the adiabatic film effectiveness are compared with an established correlation for the slot injection in Fig. 9. Taslim et al. [3] summarized the results of their parametric experimental study and proposed a general correlation of film effectiveness for the tangential slot injection. In the higher blowing ratios ($M=1.0$ and $M=2.0$), the present results agree fairly well with the correlation, though the agreement is not complete. The case of the lowest blowing ratio clearly gives a different trend from the other two cases, and consequently, there is an obvious discrepancy with the correlation. The comparisons suggest that the film behavior on the concave surface downstream of the large step is quite similar to the one well theorized on a simpler tangential slot injection when the coolant has enough momentum.

Figure 10 shows comparisons between the measured film effectiveness and the numerical results for $M=0.3$, $M=1.0$, and $M=2.0$, respectively. The comparison for $M=0.3$ indicates reasonably good agreement between the experiment and the computation. The other higher blowing ratio cases, however, show considerable discrepancies. For $M=1.0$, the computation overpredicts throughout the surface. The discrepancy is slightly reduced in $M=2.0$, but yet, it still suffers a noticeable overprediction, especially downstream. With higher blowing ratios, more coolant tends to lift-off and penetrate beyond the boundary layer. If the flow mixing outside the boundary layer is underpredicted in such a case, it will lead to an overestimation of the film effectiveness. The eddy viscosity turbulence modeling applied in the present study is probable to induce the underprediction of mixing in the mainflow region. The underprediction of mixing is from several sources: disability in capturing anisotropic nature of the diffusion, lack of terms to model the effect of streamline curvature on the turbu-

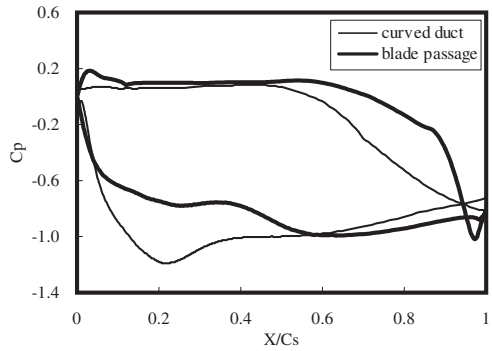

Fig. 7 Comparison of static pressure coefficient between the curved duct and the blade passage (numerical results)

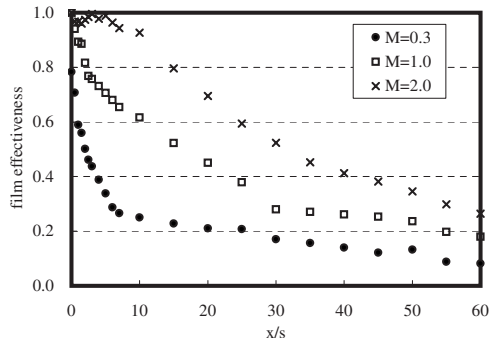

Fig. 8 Streamwise distribution of the measured centerline film effectiveness with different blowing ratios

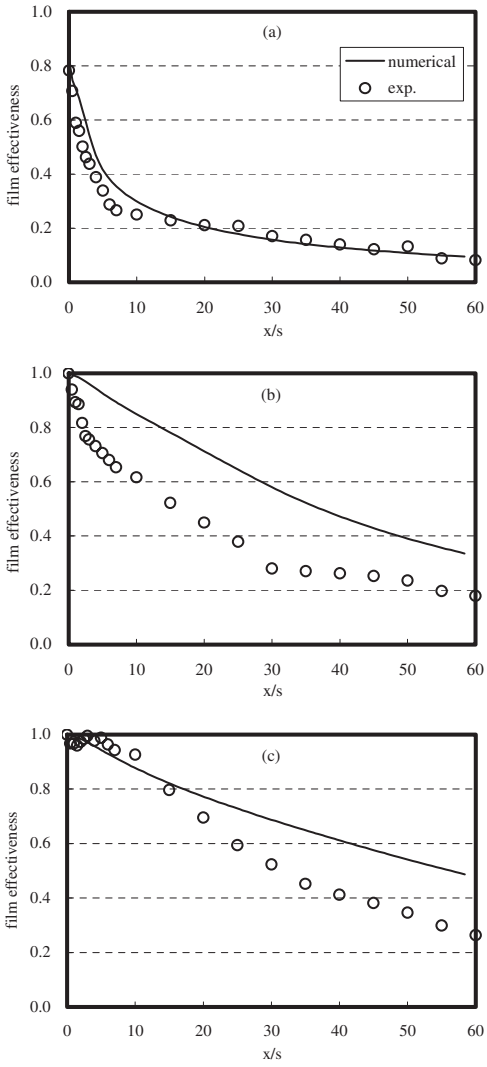

Fig. 10 Comparison of streamwise distribution of the centerline film effectiveness with different blowing ratios

lence field, etc. Also the unsteadiness in the mainflow could play an important role in higher blowing ratio conditions, while it is clearly beyond the ability of the applied numerical method.

The measured contours of the spatial thermal field in the duct and those predicted are shown in Figs. 11 and 12, respectively. For the $M=0.3$ case, both measurement and calculation show that the coolant cannot achieve an effective film layer along the surface downstream. A striking feature in this lowest blowing case is that the coolant seems to flow upstream of the slot exit. The reason of this unusual behavior, however, is understood by the computed velocity vectors plot presented in Fig. 13 (note that the plot skips every two vectors to simplify the picture). Because of the characteristic step on the concave side of the duct, an extensive separation bubble is formed near the injection point. Naturally, the convection and diffusion of the ejected coolant are affected by this recirculation flow, especially in a case where the coolant momentum is not enough. In such a case, the ejected coolant encounters the backward mainflow and is prevented from penetrating downstream. And furthermore, the coolant is swept upstream along the duct surface. Even in the higher blowing ratios (Figs. 13(b) and 13(c)), there still exists a recirculation vortex downstream the step. The point of separation is not affected by varying the blowing ratio. The whole size of the separation vortex, however, is slightly decreased and more confined behind the step when the blowing ratio is increased.

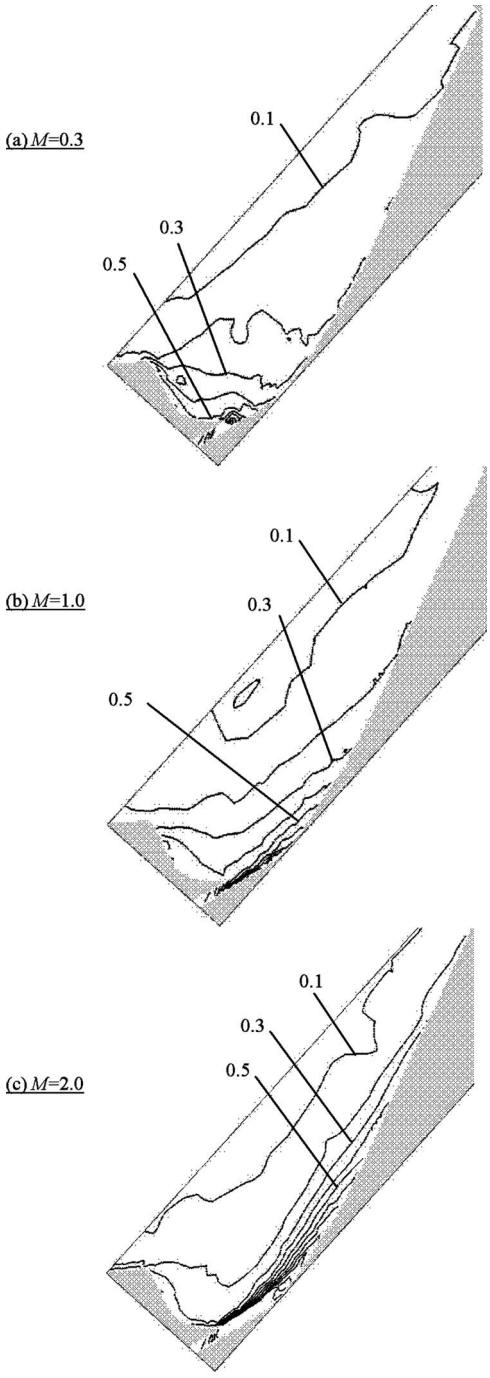

Fig. 11 Measured contours of the spatial thermal field (θ) in the duct with different blowing ratios

The measured thermal contours for the higher blowing cases (Figs. 11(b) and 11(c)) show that the coolant still has left some traces upstream of the slot opening in spite of the elevated coolant momentum, while it is not reproduced well in the computations. Both the experiment and the computation for the three blowing cases show that the film attachment and extension downstream on the concave surface are much improved in proportion to the amount of injection. The film coverage in the computation seems somewhat overestimated for the $M=1.0$ case, and this observation agrees with the trend previously shown in the comparison of the adiabatic film effectiveness. For $M=2.0$, the measured and the predicted thermal fields agree fairly well.

One of the important knowledge learned in the present funda-

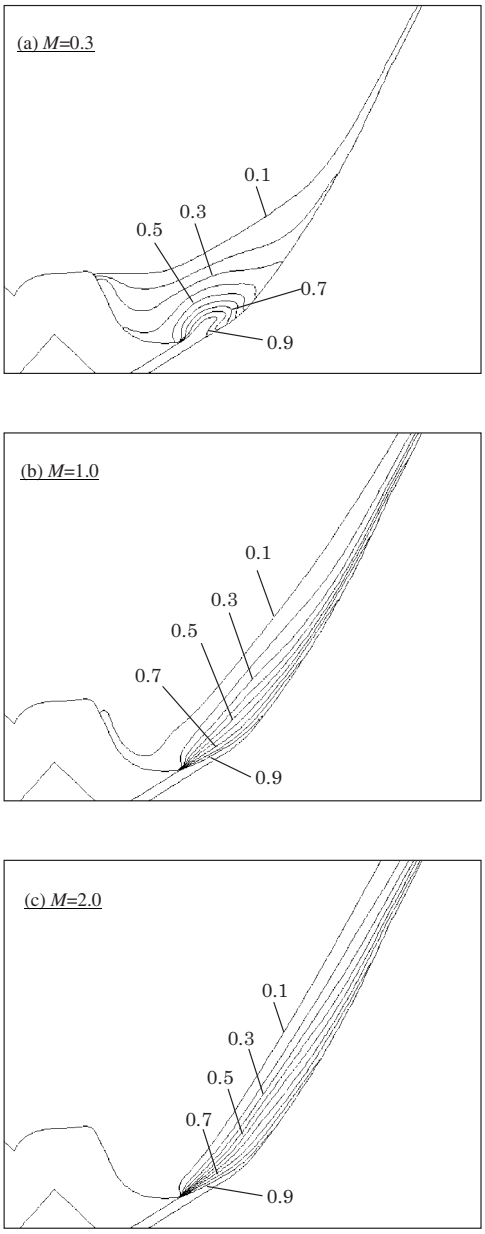

Fig. 12 Predicted contours of the spatial thermal field (θ) in the duct with different blowing ratios

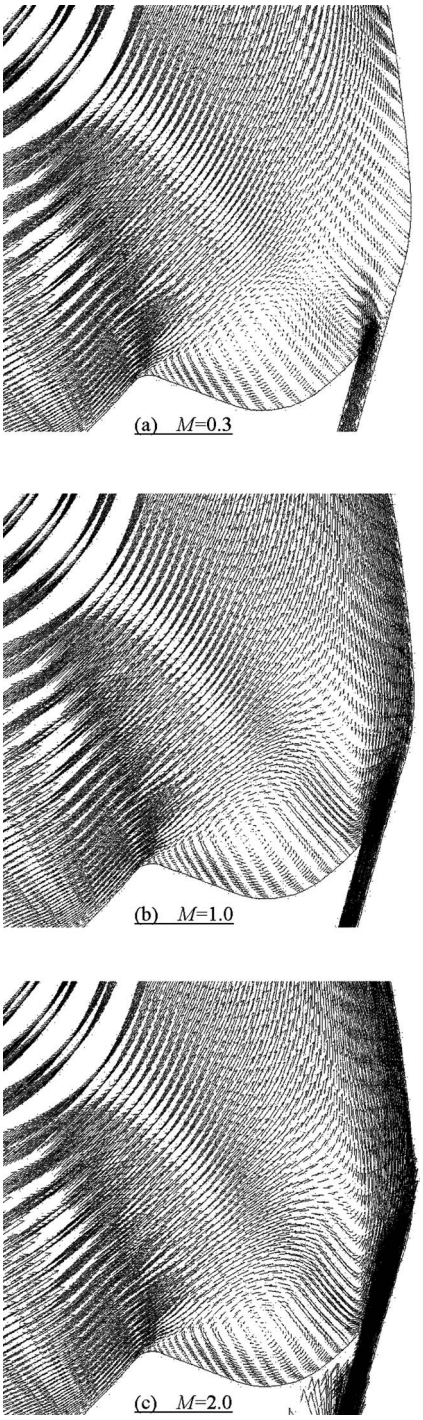

Fig. 13 Calculated velocity vectors near the film coolant injection

mental study with the curved duct is that the slot film injection is still an effective measure of cooling even in the vastly separated region, and it behaves quite similarly to the correlation organized with the simple tangential slot injection. The deviation occurs, however, in lower blowing ratios, where the thermal field is rather dominated by the intense recirculation flow, which is a distinctive feature induced by the present geometry. Another important observation is that an affordable RANS simulation is useful to investigate the detailed physics for this flow field. While quantitative agreement with the experiment is far from complete, the computational results do capture most of the important flow features. Hence, the numerical method is supposed applicable to explore the parameter space in the design optimization process.

3 Lightweight Blade Under Engine Condition

The result with the fundamental curved duct setup proves the cooling concept and the promising ability of the numerical method in simulating the flow field. Then, as a next step, the heat and the fluid flow in a blade-to-blade passage under a typical engine condition are numerically investigated.

3.1 Numerical Method. The numerical method used in the simulation around the lightweight blade is mostly same as the one for the curved duct previously mentioned. Only the differences from the previous case are summarized in this section.

The computational domains are three-dimensional because discrete film holes and/or bypass holes have to be included in the solution domain, though only one-half of the hole pitch is mod-

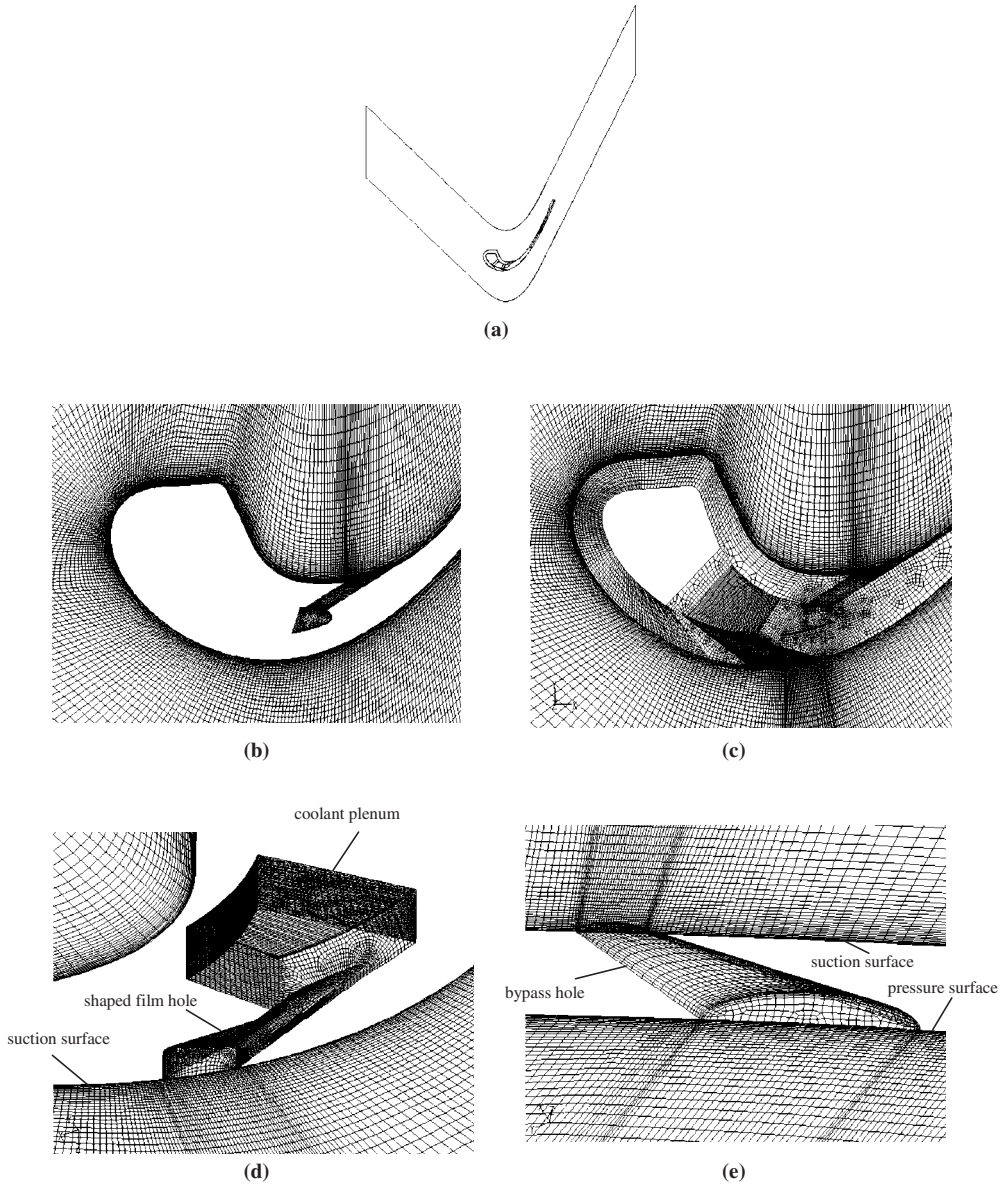

Fig. 14 Computational domain and mesh around the lightweight blade

eled in the spanwise direction. The flow around the blade is calculated in the stationary frame of reference, and the effect of rotation on the flow field is not considered in the present work.

Figure 14(*a*) shows the cross section of the whole solution domain. Two types of computations are carried out: the one only with the flow field (Fig. 14(*b*)) and the other with both fluid and solid region in a conjugate manner (Fig. 14(*c*)). Note that some internal passages of less relevance to the main interest are excluded from being directly resolved in the conjugate model. Instead, these are modeled by applying appropriate boundary conditions to simplify the calculation without loosing realistic thermal field. A discrete shaped film hole on the suction side (Fig. 14(*d*)) and/or a bypass hole through the blade (Fig. 14(*e*)) are included in addition to the slot film injection on the pressure surface. The pitch-to-throat diameter ratios for the suction-side film hole and for the bypass hole are about 3.7 and 6.5, respectively. Also the expansion and the contraction area ratio for these two types of hole are about 2.1 and 9.0, respectively.

In the computational models, only one-half of the hole pitch is solved in the spanwise direction, assuming flow symmetry with symmetry conditions being imposed at the longitudinal centerline of the hole, as well as the line between the holes. This boundary setting assumes that the holes are lined up with a constant pitch in the spanwise direction. Also the solution domain is confined to one blade pitch in the tangential direction with periodic boundary condition at the corresponding boundaries. For the cases only with the fluid, no-slip and adiabatic conditions are applied on the solid surfaces. In the conjugate cases, the fluid-solid interfaces are modeled in a conjugate manner, except for the surfaces of some internal passages, where a typical heat transfer coefficient with a prescribed coolant temperature is applied.

All the boundary condition settings are intended to simulate flow parameters in a generic HP-turbine blade. The flow parameters in the calculation are listed in Table 2. Regarding the definition of the blowing ratio, the mainflow values are based on the isentropic condition at the slot or the hole opening position in the case without any coolant blowing, and the coolant values are based on the condition at the throat section. At each coolant plenum inlet, the mass flux is set uniformly so as to give the required mass flow, and the total temperature is set at the coolant supply temperature. In the mainflow, the total pressure and the total temperature are specified at the inlet. The turbulent kinetic energy is

Table 2 Key dimensions and flow parameters in the lightweight blade simulation

	Present	Typical in engine
σ	1.3	1.0–1.5
M_{ex}	0.8	0.8–1.2
Re_{ex}	2.5×10^5	10^5-10^6
ρ_c/ρ_g	1.8	1.2–2.0
M	0.5–2.0	0.5–2.0
Bi	0.08	≈0.1

set with a turbulence intensity of 7% and the dissipation rate then obtained assuming turbulence Reynolds number equal to 100. Typically, combustor-generated, free-stream turbulence levels are around 15–20% at the first-stage vane leading edge, and due to acceleration of flow in the vane passage, the turbulence intensity at the first-stage rotor blade leading edge is typically around 5–10%. The boundary condition at the mainflow exit is same as in the previous duct case. The Biot number of the present case in Table 2 shows a value averaged over the rear part of the pressure surface in the conjugate calculations, while the corresponding typical number shows a value averaged over the entire surface of the blade in typical engines.

The number of control volume cells is about 3.6×10^4 for the cases only with the fluid, and 1.8×10^6 for the conjugate cases. The converged solutions have near-wall mesh y^+ values less than 5 in most regions. For one of the cases only with the fluid, a finer 1.2×10^5 mesh is also tested to check grid sensitivity. The streamwise distributions of film effectiveness obtained with the two grids are practically identical, as shown in Fig. 15. In the subsequent plots, the results with 3.6×10^4 mesh are presented for these cases.

3.2 Results and Discussions

3.2.1 Aerodynamics and Heat Transfer Without Film Cooling. Prior to discussing the thermal results with film cooling, the basic aerodynamics and heat transfer of the lightweight blade without film blowing is first addressed in this subsection. The proposed lightweight turbine airfoil represents a substantial departure from the conventional airfoil. In this concept, the traditional wisdom of maintaining attached flows in the turbine is cast aside to permit a lightweight geometry. Consequently, many engineering aspects are affected. Of these aspects, the first consideration is that any turbine airfoil has to provide the required aerodynamic performance. Also, the thermal behavior, where the main interest of this paper exists, and structural integrity are intimately related to the aerodynamic performance.

Figure 16 compares the computed isentropic surface Mach number between the conventional airfoil (shown in Fig. 1) and the lightweight airfoil. Both airfoils are designed with identical aerodynamic loading. In the lightweight airfoil, there is a slight deceleration at about $X/Cs=0.4$ on the suction surface, and there is also a similar dip on the pressure surface ($X/Cs=0.55$), which both may cause unfavorable aerodynamic effects. Comparing to the conventional airfoil, the diffusion region in the rear part of the suction surface is shorter with the lightweight airfoil. Also, the peak Mach number on the suction surface is decreased with the lightweight airfoil. Obviously it is better to decrease the peak Mach number to reduce the profile loss. In a modern LP-Turbine design, the lower peak Mach number is realized by applying thinner airfoil. With the conventional cooled HP-Turbine blade, however, it is difficult to apply the same approach.

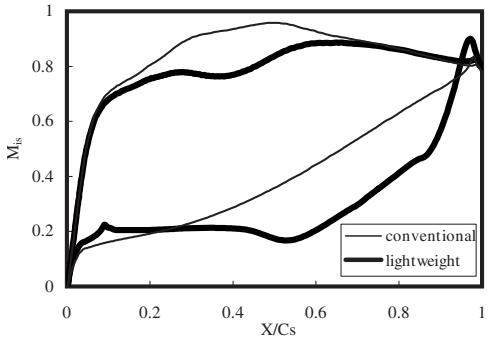

Fig. 16 Computed isentropic surface Mach number profiles with the conventional and the lightweight airfoils

Figure 17 shows the pitchwise profile of the computed loss coefficient at two different sections downstream of the cascade. The definition of the loss coefficient is $(p_{t,\text{in}}-p_t)/(p_t-p)$. Both airfoils show almost the same profile and magnitude of the pressure loss at the two sections. With the lightweight airfoil, the flow separates on the pressure surface, but reattaches; therefore, the additional loss increase by the separation can be kept minimal. On the other hand, the lower peak Mach number and the shorter diffusion region on the suction surface aforementioned will have positive consequences. As a whole, the pressure loss with the lightweight airfoil is comparable to the conventional airfoil at least in the two-dimensional aerodynamics.

If the flow separates, but reattaches, then one would expect such a flow field to have a substantial impact on the convective heat transfer characteristics on the pressure side. Figure 18 compares the computed heat transfer coefficient along the pressure surface between the two airfoils. The heat transfer coefficient is normalized by the base value of fully turbulent boundary layer over flat plate with $Re=2.5\times10^5$. In the lightweight design, an extremely low heat transfer in the separation bubble and a subsequent gradual increase downstream of the separated region are observed. Though a considerable elevation of the heat transfer

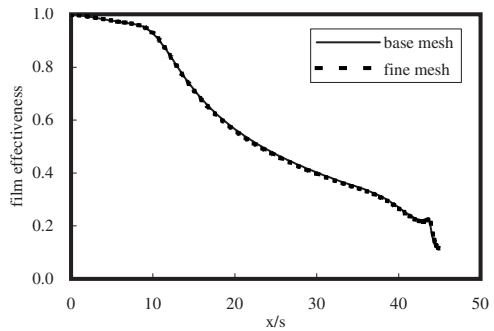

Fig. 15 Comparison of streamwise distribution of calculated film effectiveness with the two grids for $M=1.0$

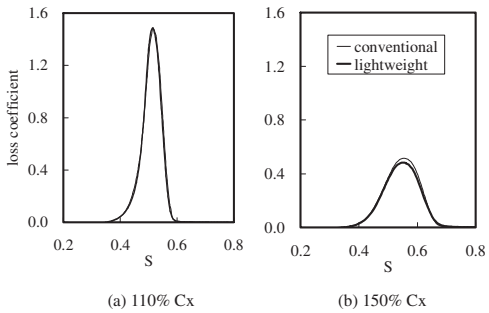

Fig. 17 Pitchwise distribution of computed loss coefficient with the conventional and the lightweight airfoils

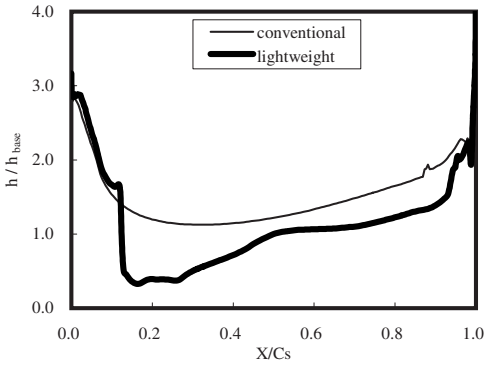

Fig. 18 Heat transfer coefficient on the pressure surface with the conventional and the lightweight airfoils

occurs in the reattachment region, the level over the rear part of the pressure surface is still sensibly lower than the conventional airfoil.

3.2.2 Effect of Pressure-Side Film Cooling. Regarding the thermal field with film cooling, a case only with the pressure-side film cooling is first investigated. This configuration is most relevant to the flow field studied in the experimental setup. Figure 19 shows a comparison of the streamwise distribution of the calculated film effectiveness with the three different blowing ratios. Note that the lowest blowing ratio value (0.5) is slightly higher than the value studied in the experiment. The overall trend is very similar to the experiment; a positive dependence on the blowing ratio with particularly poor cooling performance in the lowest blowing ratio.

The calculated thermal field around the blade depicted in Fig. 20 also demonstrates that the important flow features observed in the low speed experiment are mostly reproduced in the actual engine condition. The insufficient film adherence with the $M=0.5$ case is reasonably understood by a clear evidence of backward flow of the coolant. The ejected coolant is less susceptible to the mainflow as its momentum increases. Although the extensive mixing in the pressure-side dip enhanced by the recirculation vortex is evident even with the higher blowing ratios, the sufficient coolant injection on the surface proves to be an effective cooling measure for the proposed blade shape.

3.2.3 Combined Effect of Pressure-Side and Suction-Side Film Cooling. The next step is to study the overall cooling system and to optimize the design. With the proposed blade concept, the front part of the blade has internal coolant paths; therefore, any proven cooling strategy (e.g., roughened serpentine paths with a showerhead in the leading edge) can be applied. The stumbling block of this concept is clearly the rear part of the blade, so the optimization effort is primarily made to this region.

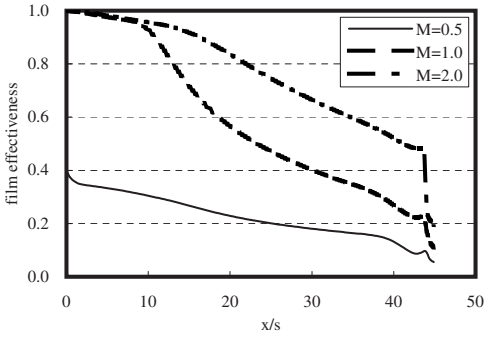

Fig. 19 Comparison of streamwise distribution of calculated film effectiveness with different blowing ratios

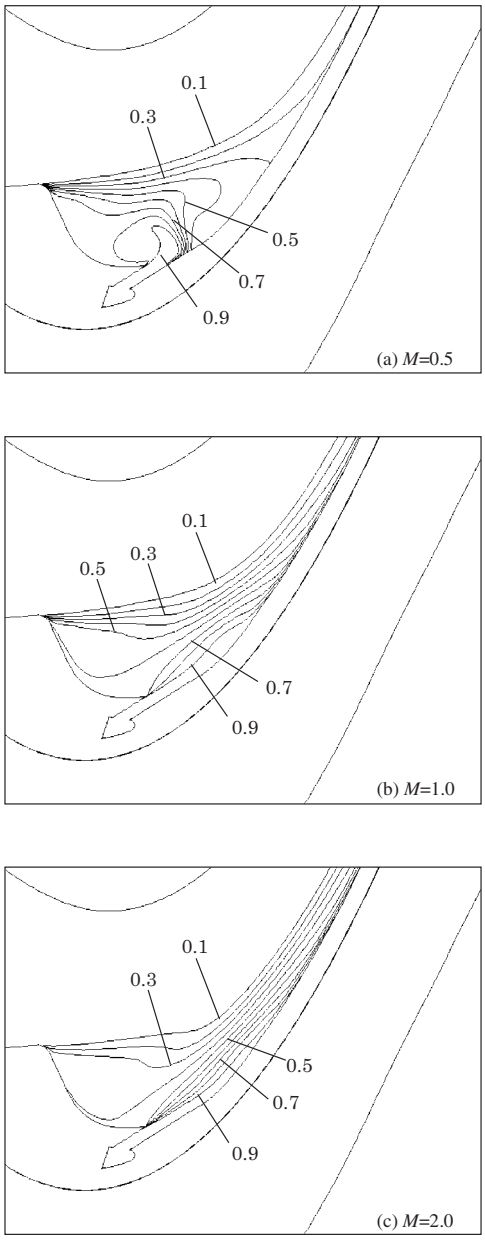

Fig. 20 Predicted contours of temperature (θ) around the lightweight blade with different blowing ratios

On the pressure side, the film cooling is already considered. Only the available cooling option to be applied on the suction side of this blade is also the film cooling. Under the present study, the suction-side film coolant is designed to be ejected from the middle internal cavity of the blade (see Fig. 14(*d*)).

To evaluate the direct effect of the cooling design on the resultant component metal temperature, conjugate simulations are carried out for the following cases. With the present cooling system, the front part of the blade is expected to follow the standard design correlation and also is not the main interest of the current study; therefore, the thermal boundary conditions in that region are simplified without being fully resolved in the conjugate manner.

Figure 21 shows the calculated thermal field in the centerline section of the suction-side film hole and in the section halfway between the holes with the two different blowing ratios (1.0 and 2.0) for the suction-side film cooling injection. For the pressure-

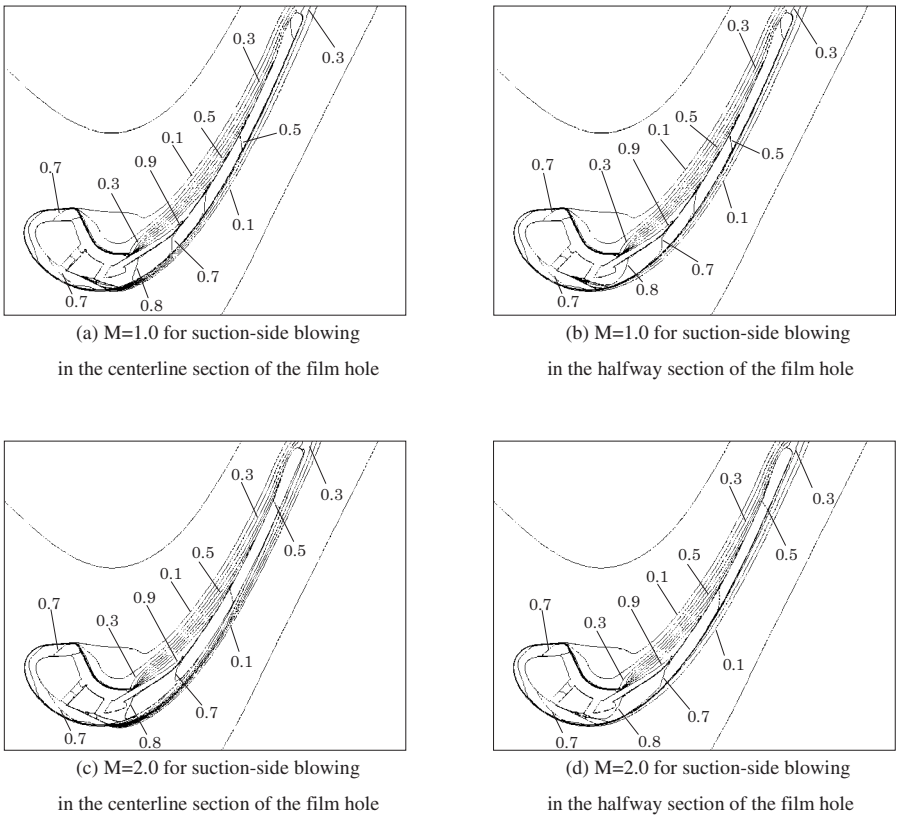

(a) M=1.0 for suction-side blowing in the centerline section of the film hole

(b) M=1.0 for suction-side blowing in the halfway section of the film hole

(c) M=2.0 for suction-side blowing in the centerline section of the film hole

(d) M=2.0 for suction-side blowing in the halfway section of the film hole

Fig. 21 Predicted contours of fluid and solid temperature (θ) with pressure-side and suction-side film cooling (M=2.0 for pressure-side blowing)

side film cooling, the fixed blowing ratio of 2.0 is applied because of the highest cooing performance within the investigated blowing range.

Any noticeable difference in the thermal field cannot be seen between the centerline and the halfway sections, except for the region close to the hole exit. Comparing the two blowing cases, the higher blowing ratio on the suction side contributes to the lower metal temperature. The differences in the normalized temperature between the two blowing ratio cases are on the order of 0.1 in the rear part of the blade. The coolant film on the suction side is well attached to the surface for the both blowing ratios. Even with the higher blowing ratio, a blowoff of the coolant jet is not predicted with the present simulation. The trailing edge portion is inevitably most critical in the temperature for both cases. An important feature in the thermal field is that the pressure side is constantly cooler than the suction side at each location of the rear part. A possible reason is that the total amount of the ejected film coolant is larger on the pressure side than on the suction side, since the two-dimensional slot film is assumed on the pressure side, whereas the discrete film holes on the suction side. Thermal gradient across the blade thickness is slightly larger for $M=1.0$. Therefore, from the point of view of induced thermal stress, the higher blowing ratio on the suction side is better, though a centrifugal force usually dominates the overall stress field for a rotating blade.

3.2.4 Introduction of Bypass Cooling Hole. The results with the pressure- and suction-side film cooling suggest the possibility of excessive cooling on the pressure side with the present cooling system. In other words, the coolant is used more than is necessary, and there is still a room to optimize the cooling design. A straightforward solution is to reduce the blowing ratio on the pressure surface. However, less film coolant on the recirculating pressure side may lead to a significant deterioration in the cooling performance as mentioned in the previous sections.

One of the other alternatives studied in the present work is to bypass some of the film coolant from the pressure side to the suction side through discrete holes (as shown in Fig. 1) while keeping the higher blowing ratio on the pressure surface.

One concern about bleeding the coolant to the rear portion of the suction surface is a detrimental effect on the aerodynamic performance. The surface Mach number on this region is usually highest around the blade, and an introduction of the secondary fluid in such a high-speed region results in a considerable increase in the mixing loss. To avoid this, the proposed bypass hole is shaped like a convergent nozzle, as shown in Fig. 14(*e*). The aim of this hole shaping is to accelerate the coolant through the hole, and then, to minimize the shear stress in the boundary layer on the issued suction surface. The convergent hole may not achieve high film effectiveness as a divergent fan shaped hole exhibits, but yet it provides the best solution when both the aerodynamic efficiency and the cooling performance are optimized in this critical region. For a hollow blade, such a convergent hole shape is very expensive to manufacture by laser drilling or electro discharge machining. With the current blade concept, however, it can be much easily drilled by any of these machining methods.

In the present study, two different chordwise locations are investigated for the bypass hole, that is, 77% and 67% of the suction-side surface length. The spanwise location of the bypass hole is half-pitch staggered with the suction-side film hole.

Figure 22 compares the calculated thermal field in the centerline section of the bypass hole and in the section halfway between the holes with the two different bypass hole locations. The blowing ratio of the pressure-side and of the suction-side blowing is $M=2.0$ and $M=1.0$, respectively.

Again, any noticeable difference in the thermal field cannot be seen between the centerline and the halfway sections, except for

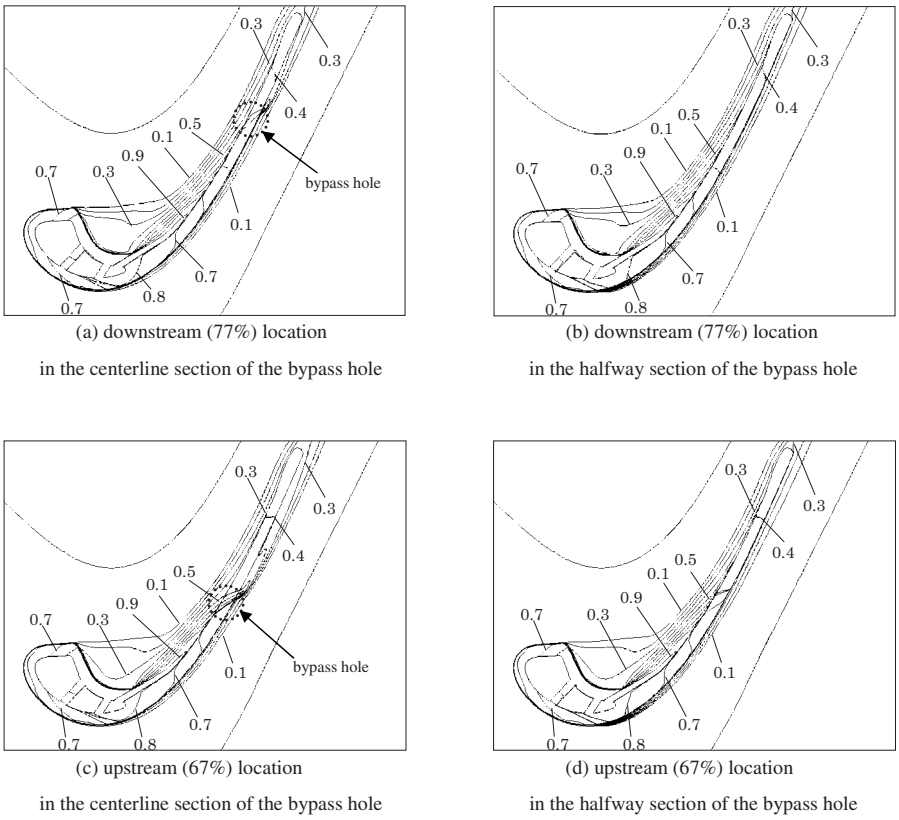

(a) downstream (77%) location in the centerline section of the bypass hole

(b) downstream (77%) location in the halfway section of the bypass hole

(c) upstream (67%) location in the centerline section of the bypass hole

(d) upstream (67%) location in the halfway section of the bypass hole

Fig. 22 Predicted contours of fluid and solid temperature (θ) with two different bypass hole locations (M=2.0 for pressure-side blowing and M=1.0 for suction-side)

the region near the bypass hole. The figure shows that the bypass hole effectively works as being intended. The film coolant on the pressure surface is partly bled and provided to the rear portion of the suction surface through the bypass hole. On the suction surface, the bypassed coolant is piled on the existing film layer. Compared with the case without the bypass hole (Figs. 21(*a*) and 21(*b*)), the introduction of the bypass hole contributes to a reduction in the thermal gradient across the blade thickness in the trailing edge region, especially with the case of upstream (67%) location. The coolant through the bypass hole is driven by the pressure difference across the blade. Locating the hole upstream increases the amount of bypassed coolant, and as a result, the balance of the film cooling performance between the pressure side and the suction side is more changed.

Before concluding the discussion, it is worthwhile to evaluate the total coolant amount of the final design shown in Figs. 22(*c*) and 22(*d*). The ejected coolant amount as a percentage of the mainflow at the cascade inlet is 3.1% for the pressure-side slot, and 1.0% for the suction-side film cooling hole, and the total coolant amount of this blade, including the leading edge cooling, is 5.9%. The resultant overall cooling effectiveness shown in Figs. 22(*c*) and 22(*d*) is about η=0.66. The typical coolant amount to achieve this level of cooling performance with conventional cooling strategy (e.g., rib-roughened multi-internal paths with several discrete rows of film cooling externally) is estimated around 6–7%. Therefore, the present design result can stand in comparison with the conventional design regarding the cooling performance.

4 Conclusion

To investigate the feasibility of a novel lightweight cooled turbine blade, a separated flow field with film cooling is studied in a curved duct experiment. Numerical calculations are also carried out to understand the physics of this unique flow field. The calculated film effectiveness and the thermal field are thoroughly compared with the experimental data to verify the numerical modeling. With the numerical measure, cooling performance of the proposed blade under a typical engine operating condition is predicted. There are several important conclusions to be made from the present work.

1. The slot film injection is an effective measure of cooling even in the vastly separated region. It behaves quite similarly to the correlation organized with the simple tangential slot injection. The deviation occurs, however, in lower blowing ratios, where the thermal field is rather dominated by the intense recirculation flow.
2. Numerical flow simulation with a RANS-level modeling is useful to investigate the detailed physics for this type of flow field. While quantitative agreement with the experiment is far from complete, the computational results do capture most of the important flow features.
3. Numerical calculations of the proposed blade under a typical engine condition suggest that the overall flow patterns and the resultant film coolant behavior in the pressure-side separated region observed in the low speed experiment are mostly reproduced in the blade-to-blade flow field under the transonic design condition.
4. The conjugate simulation of the entire blade shows that the trailing edge portion is most critical in the temperature and the thermal gradient across the blade thickness is large. It is numerically demonstrated that the idea of bypassing film coolant from the pressure side to the suction side is effective in controlling the thermal gradient across the airfoil and in optimizing the overall temperature distribution of the blade.

The present work brings about the promising results with the novel turbine blade, even if it is still in a fundamental research

phase. The next step will be a stationary cascade test and a rotating rig test in order to verify the aerodynamic and thermal performance, especially at off-design conditions. In parallel with the performance evaluation in the rig test, other structural concerns (e.g., vibration issues, especially the flutter problem attended with the less rigid airfoil) will be also investigated by numerical and experimental measures.

Nomenclature

- Bi = Biot number, ht/λ
- c = chord length
- Cp = static pressure coefficient, $(p-p_{\mathrm{in}})/(p_{t,\mathrm{in}}-p_{\mathrm{ex}})$
- Cs = chord length along the surface from leading to trailing edge
- Cx = axial chord length
- H = step height
- h = duct height or heat transfer coefficient, $q_w/(T_w-T_{aw})$
- h_{base} = heat transfer coefficient of the fully turbulent boundary layer over flat plate
- M = blowing ratio, $(\rho U)_c/(\rho U)_g$, or Mach number
- $\mathrm{M_{is}}$ = isentropic surface Mach number
- p = static pressure
- p_t = total pressure
- q_w = heat flux
- $\mathrm{Re_{ex}}$ = Reynolds number at the cascade exit, $\rho U_{\mathrm{ex}} c/\mu$
- Re_s = slot Reynolds number, $\rho U s/\mu$
- Re_θ = Reynolds number based on boundary layer momentum thickness, $\rho U\theta/\mu$
- S = normalized coordinate in the pitchwise direction
- s = injection slot height
- T = temperature
- t = slot lip thickness or blade thickness
- U = velocity
- w = duct width
- X = coordinate along the surface from leading edge
- x = coordinate along the surface from slot exit
- y = coordinate normal to the wall
- α = injection angle
- η = cooling effectiveness, $(T_g-T_m)/(T_g-T_c)$
- η_f = adiabatic film effectiveness, $(T_g-T_{\mathrm{aw}})/(T_g-T_c)$ (for curved duct setup) and $(T_{\mathrm{aw},0}-T_{\mathrm{aw}})/(T_{\mathrm{aw},0}-T_c)$ (for transonic condition)
- λ = thermal conductivity
- μ = viscosity
- ρ = density
- θ = momentum thickness or normalized temperature, $(T_g-T)/(T_g-T_c)$
- σ = solidity

Subscripts

- 0 = without film blowing
- aw = adiabatic wall
- c = coolant
- ex = cascade exit
- g = mainflow
- in = cascade inlet
- m = surface of the component
- w = uniform heat flux wall

References

[1] Calzada, P., and Alonso, A., 2002, "Numerical Investigation of Heat Transfer in Turbine Cascades With Separated Flows," ASME Paper No. GT-2002-30225.

[2] Yamawaki, S., 2005, "Thin-Walled, Lightweight Cooled Turbine Blade," U.S. Patent No. 6926499.

[3] Taslim, M. E., Spring, S. D., and Mehlman, B. P., 1992, "Experimental Investigation of Film Cooling Effectiveness for Slots of Various Exit Geometries," J. Thermophys. Heat Transfer, **6**(2), pp. 302–307.

[4] Holloway, D. S., Leylek, J. H., and Buck, F. A., 2002, "Pressure-Side Bleed Film Cooling: Part 1—Steady Framework for Experimental and Computational Results," ASME Paper No. GT-2002-30471.

[5] Holloway, D. S., Leylek, J. H., and Buck, F. A., 2002, "Pressure-Side Bleed Film Cooling: Part 2—Unsteady Framework for Experimental and Computational Results," ASME Paper No. GT-2002-30472.

[6] Martini, P., Schulz, A., and Wittig, S., 2003, "Experimental and Numerical Investigation of Trailing Edge Film Cooling by Circular Coolant Wall Jets Ejected From a Slot With Internal Rib Arrays," ASME paper GT-2003-38157.

[7] Martini, P., Schulz, A., and Bauer, H.-J., 2005, "Film Cooling Effectiveness and Heat Transfer on the Trailing Edge Cut-Back of Gas Turbine Airfoils With Various Internal Cooling Designs," ASME Paper No. GT2005-68083.

[8] Kim, Y. W., Coon, C., and Moon, H.-K., 2005, "Film-Cooling Characteristics of Pressure-Side Discharge Slots in an Accelerating Mainstream Flow," ASME Paper No. GT2005-69061.

[9] Cunha, F. J., Dahmer, M. T., and Chyu, M. K., 2005, "Analysis of Airfoil Trailing Edge Heat Transfer and Its Significance in Thermal-Mechanical Design and Durability," ASME Paper No. GT2005-68108.

[10] Okita, Y., Nakamata, C., Kamiya, H., and Kumada, M., 2005, "Film Cooling for Slot Injection in Separated Flows," ASME Paper No. GT2005-68119.

[11] Kline, S. J., and McClintock, F. A., 1953, "Describing Uncertainties in Single-Sample Experiments," Mech. Eng. (Am. Soc. Mech. Eng.), **75**(1), pp. 3–8.

[12] 2006, FLUENT Version 6.3, Fluent Inc., New Hampshire.

[13] Kacker, S. C., and Whitelaw, J. H., 1969, "An Experimental Investigation of the Influence of Slot Lip Thickness on the Impervious Wall Effectiveness of the Uniform Density, Two Dimensional Wall Jet," Int. J. Heat Mass Transfer, **12**, pp. 1196–1201.

[14] Burns, W. K., and Stollery, J. L., 1969, "The Influence of Foreign Gas Injection and Slot Geometry on Film Cooling Effectiveness," Int. J. Heat Mass Transfer, **12**, pp. 935–951.

[15] Bittlinger, G., Schulz, A., and Wittig, S., 1994, "Film Cooling Effectiveness and Heat Transfer Coefficients for Slot Injection at High Blowing Ratios," ASME Paper No. 94-GT-182.